Chemistry during the early phases of star formation

Chamilla Terp (bmx626)

Computational Astrophysics Exam Project, 14th to 17th of January 2025

1 Introduction

In modern astrophysics, low-mass stars are understood to form in dense molecular clouds through gravitational collapse. These clouds, composed primarily of hydrogen molecules, are also enriched with diverse chemical species. The chemistry within them plays a crucial role in star formation, influencing the thermodynamic conditions and cooling rates that facilitate collapse. As the cloud begins to contract under the influence of gravity, its density and temperature increase, leading to the formation of the first Larson core. As temperatures rise to $\sim$ 2000 K the second Larson core, a dense, hot object dominated by atomic and ionic chemistry is formed. These chemical changes are crucial for understanding early star formation and have significant implications for planet formation and prebiotic chemistry.

This project aims to calculate the evolution of species abundances in a basic chemical network during early star formation. The chemical abundances will be computed on a background fluid, whose evolution have already been computed.

2 Numerical methods

The data used in this project was released in 2016 [3], where a number of runs/calculations were performed for the gravitational collapse of a Bonnor-Ebert like sphere. The data consists of 4059 cells, but only 40 is chosen to run the chemistry on in this project. Each run consists of a varying number of data files, and the chemical network evolution is simulated using all available files.

2.1 Numerical setup

The simulations conducted in this project incorporate a reduced chemical network for H_2O by solving a system of ordinary differential equations (ODEs) of the form (following the procedure of exercise 6):

$$\frac{dn_i}{dt} = \Sigma_{lm} k_{lm}(T) n_l(t) n_m(t) - n_i(t) \Sigma_j k_{ij}(T) n_j(t) \tag{1}$$

where k represents the reaction rate coefficient and n denotes the abundances of the reactants. Eq. 1 accounts for both the formation and destruction processes of a given species. The set of ODEs representing the chemical network is solved using the Python function `solve_ivp` form `scipy.integrate`. The network is first run for a single cell to ensure that everything works correctly before running it over a grid of cells.

2.1.1 Dynamic gas temperature, T_{gas}

Before setting up the grid and running the network, I need to take into consideration how the temperature changes at every time-step. Therefore, the functions `rate_coefficients()`, `reaction_rates()` and `differential_equations()` are changed to be temperature dependent instead of having a global T_{gas} value as in exercise 6. This temperature is passed into the solver as an `args` argument and the dynamic temperature is now taken into account.

2.1.2 Dynamic mean molecular weight, μ

The ODE solver used takes the number densities as input and not concentrations, which means that I need to scale the abundances with the total number density $n_{\text{tot}} = \frac{\rho}{\mu m_H}$, where μ is the mean atomic weight. As the concentration changes, μ also changes, which means that I need to update it while running the network. This is done by calculating the final concentration from the solution as `solution.y[:, -1] / np.sum(solution.y[:, -1])` and from this the new μ value as `np.sum (concentration * mass)`. This is used to reset the μ value after each iteration, thus ensuring that it is dynamic and follows the evolution of the network.

As seen in Figure 1, changing μ from being 2.1 during all iterations to making it dynamic, does not make a big difference. The new values for μ is ~ 2.01, and does not change the concentrations significantly.

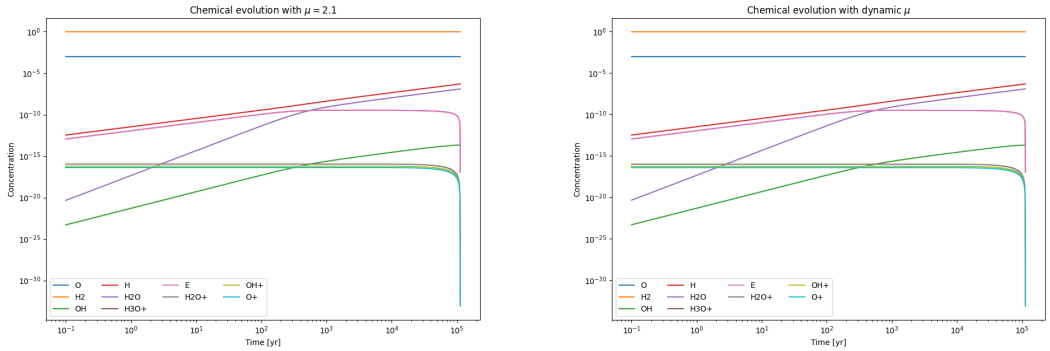

Figure 1: Chemical evolution of all species for a single cell with both fixed and dynamic μ.

2.1.3 Thermal dissociation

The initial network does not account for all physical processes. I therefore add the following thermal dissociation of H_2 molecules to the network: $H_2 + H \rightarrow H + H + H$. This is done following the same procedure from exercise 6, task 4, where the three functions `rate_coefficients()`, `reaction_rates()` and `differential_equations()` are updated to include the new reaction. The rate coefficient needed are found on the KIDA website [1]. The final chemical network with the thermal dissociation is shown in Figure 2.

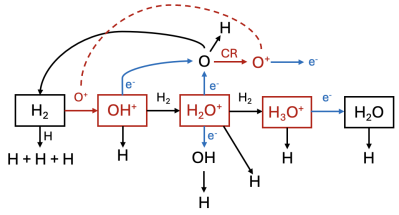

Figure 2: Chemical network with thermal dissociation included.

2.1.4 Setting up and initializing the grid for the multi-cell solver

The grid represents the chemical composition and properties of the network, where each cell corresponds to a cell with initialized species concentrations and mean molecular weights. The chemical species is mapped to indices in an 2D array. This array store the abundances of $N_{\texttt{species}}$ for each cell, where the dimensions is determined by the number of cells and species. The concentrations is then initialized to 10^{-40} (ensuring that there is no division by 0) with specific values assigned to H_2 = 1 and O_2 = 10^{-3}. Lastly, for each cell μ is calculated as the weighted sum of concentrations multiplied by species masses.

2.1.5 Setting up the multi-cell solver

After ensuring that the solver works with the implementations mentioned above, the multi-cell solver is build. First it is structured to process the data files (i.e. "snapshots" of the physical conditions at specific times) sequentially. For each file, the relevant data is extracted, including density (ρ) and gas temperature (T_{gas}). These vales are used to compute the total number density (n_{tot}) and the concentrations of the species in each cell. For each time-step, a dynamic time grid is constructed, where the time-step size is adjusted based on the duration between "snapshot" times. To ensure charge neutrality, the electron density in the grid is updated during each iteration.

The solver, `solve_ivp`, dynamically adjusts the maximum step size if a convergence issue arise, and retries until it is successful. The results, the concentration ($n/\Sigma n$) and corresponding time values, is then stored for each cell. After solving the current time-step, the final concentrations and μ are updated and used as new initial conditions for the next iteration (as described in Section 2.1.2).

3 Results

I first look at data from run 67, with t_{ff} = 48 kyr, $M_0 = 1\ M_\odot$, $T_0 = 10$ K, and $R_0 = 7500$ AU. The result where all of the steps in Section 2.1 have been implemented can be seen in Figure 3.

3.1 Abundances in different parts of the system

The plots in Figure 3 clearly illustrate the time evolution of different species across various regions of the system, corresponding to the stages of early star formation. Initially, during the pre-stellar phase, H_2 dominates, maintaining a nearly constant and high concentration throughout the evolution. This reflects the isothermal collapse phase, where molecular hydrogen is the primary coolant. Atomic oxygen (O) and electrons (E) also exhibit relatively stable abundances, driven by reactions such as cosmic-ray ionization of O to O^+. Ions like OH^+, H_2O^+, and H_3O^+ are formed through reactions with H_2, such as $O^+ + H_2 \rightarrow OH^+ + H$, $OH^+ + H_2 \rightarrow H_2O^+ + H$, and $H_2O^+ + H_2 \rightarrow H_3O^+ + H$. These reactions are particularly important during the formation of the first Larson core, where the gas begins to heat up and optical thickness increases, slowing the collapse. As the system evolves, the reactions driven by electrons begin to dominate. However, the rate coefficients of these reactions decrease with increasing temperature since they depend on $\frac{1}{\sqrt{T_{gas}/300}}$, which explains the declining abundances of H_3O^+, H_2O^+, and OH^+ at later times. Towards the end of the simulation, as the

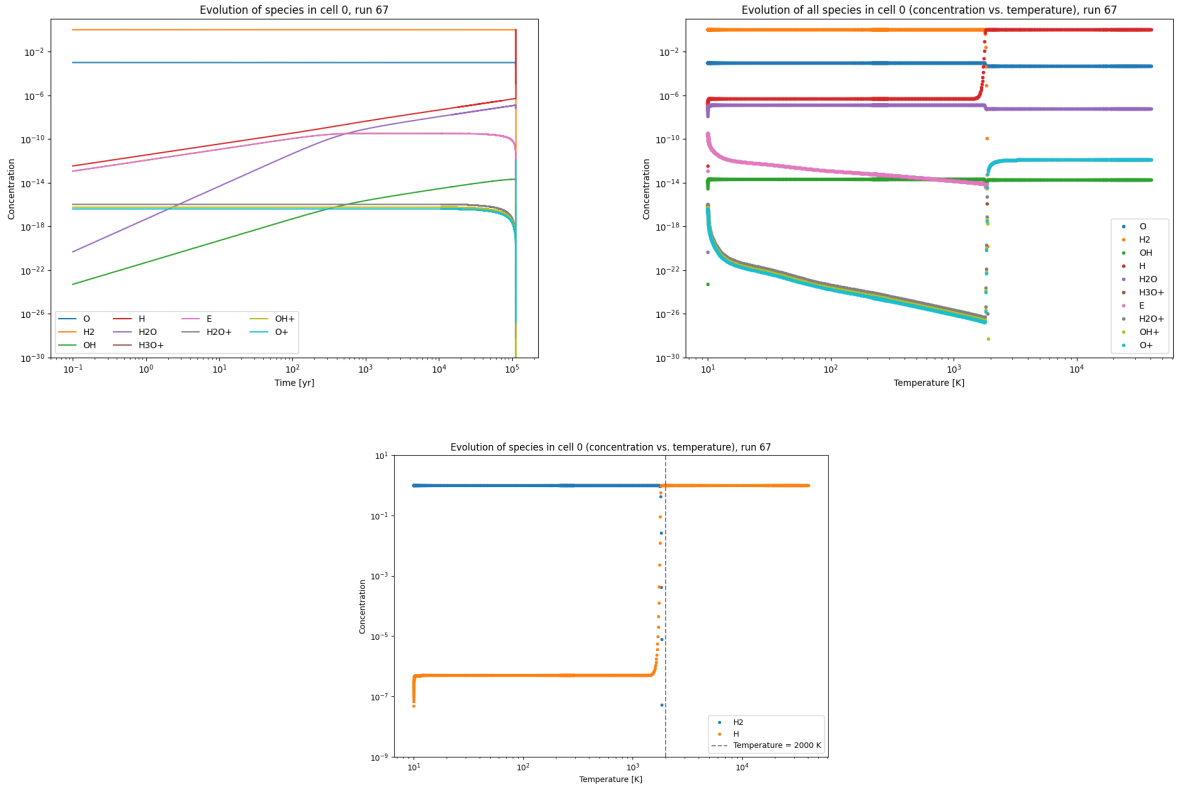

Figure 3: Different plots showing the chemical evolution from run 67.

second Larson core begins to form, neutral species like H_2, O, and H_2O remain relatively abundant, as they are less sensitive to the decreasing reaction rates at high temperatures. However, as we reach temperatures of $\sim$ 2000 K during the transition to the second Larson core, H_2 dissociates, resulting in the sharp decrease in concentration of H_2 and the liberation of atomic hydrogen (H), seen as a sharp increase in concentration. The reduction in H_2 also influences the formation of the ions and consequently, the concentrations of those decrease significantly.

3.2 Comparison of different runs - collapse time, t_{ff}

For the comparison of different initial conditions, I choose run 71 and 65. Run 70 have a collapse time $t_{ff} =$ 34 kyr, $M_0 = 2\ M_\odot$, $T_0 = 20$ K, and run 65 have $t_{ff} = 68$ kyr, $M_0 = 0.5\ M_\odot$, $T_0 = 5$ K. Both runs have the same initial radius as run 67. The results of the new runs are shown in Figures 4 and 5.

Looking at the effect of the collapse time, we can see by comparing Figures 3, 4, and 5, that a shorter collapse time leads to faster thermal evolution, resulting in sharper transitions in the concentrations of the species. The rapid progression reduces the time for reactions to establish equilibrium, leading to slightly lower concentrations final products, such as OH, H_2O, and the ions for run 71 compared to run 67 and 65. The longer collapse time in run 67 and 65 allows for a more gradual evolution, enabling higher abundances of complex molecules to form before the temperature rises. It is also clear, that for a lower collapse time the system reach the dissociation temperature faster. This is reflected in the earlier occurrence of the sharp drop in concentrations for run 71, compared to run 65 and 67.

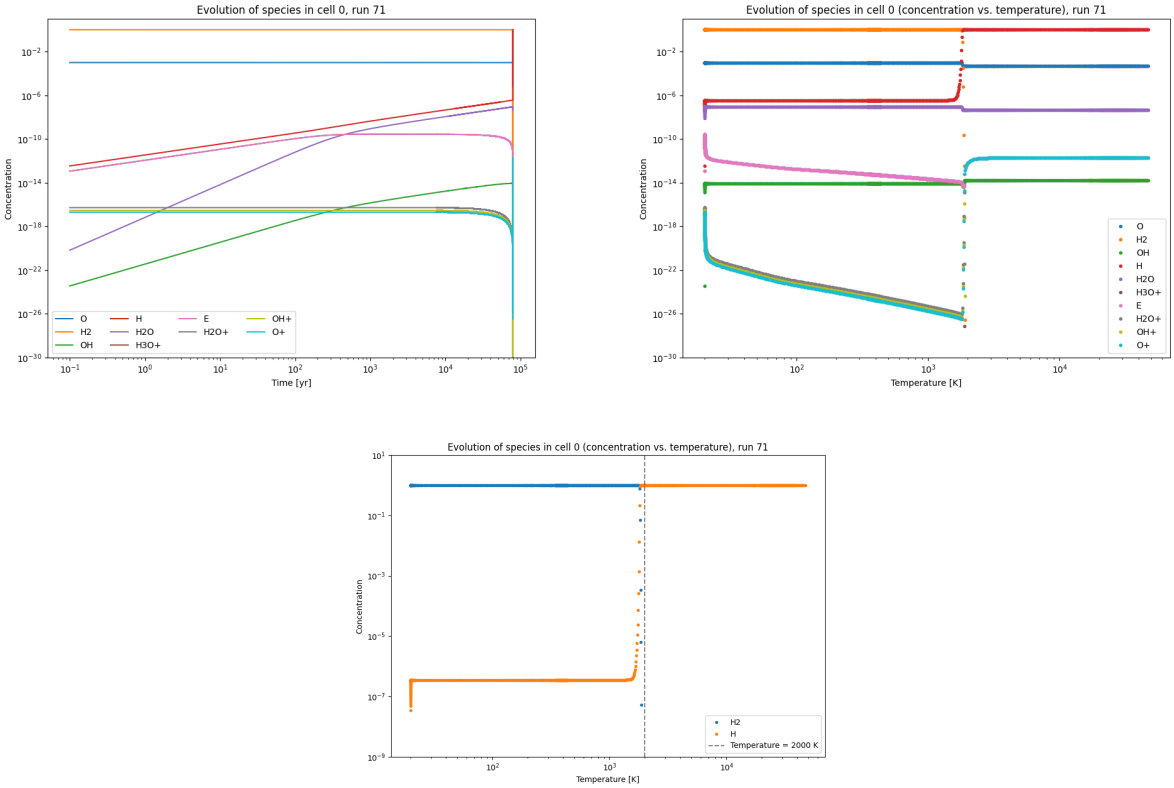

Figure 4: Different plots showing the chemical evolution from run 71.

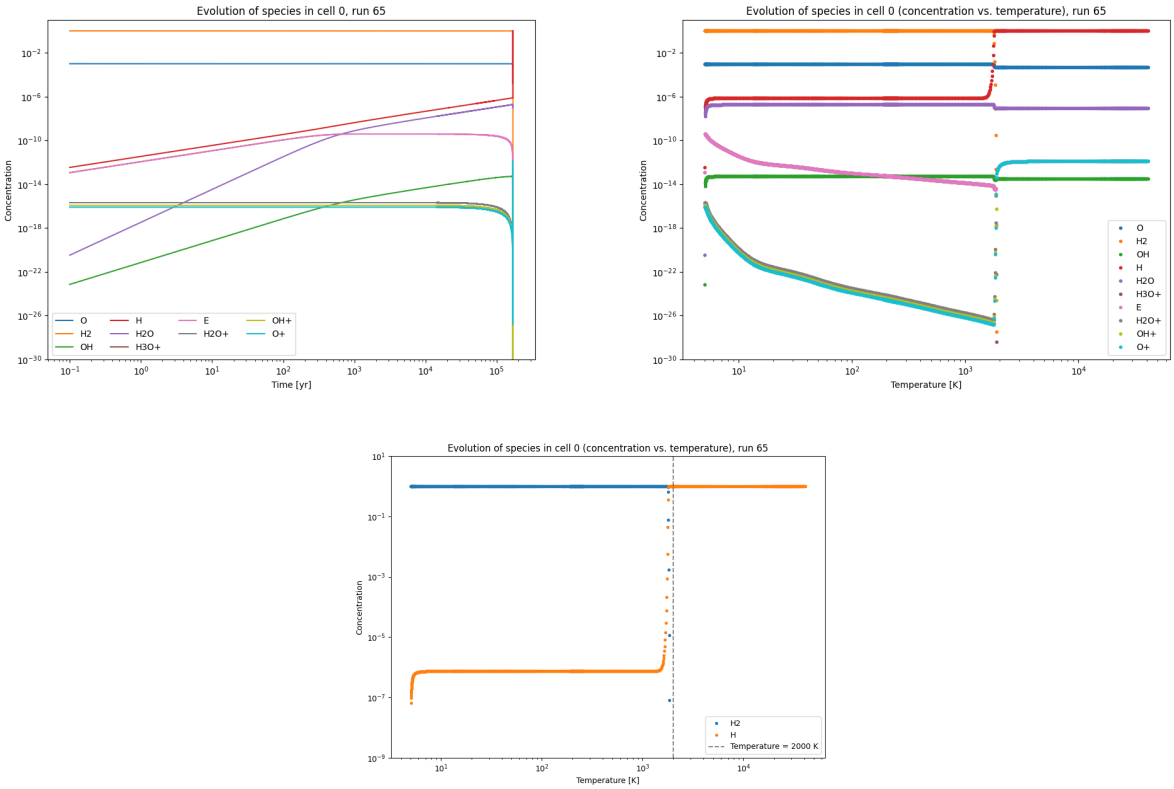

Figure 5: Different plots showing the chemical evolution from run 65.

3.3 Expanding the network

I expand the network following the same procedure as in Section 2.1.3 with the two following reactions (with rate coefficients) from Umebayashi & Nakano (1990) [2]:

$$H^+ + O \rightarrow O^+ + H \quad (k = 1.2 \times 10^{-9})$$

$$H^+ + O_2 \rightarrow O_2^+ + H \quad (k = 7.0 \times 10^{-10} \exp(-232/T_{\text{gas}}))$$

Running the simulation with run 67 yields the results shown in Figure 6. Introduction the two reactions to the network, does not seem to have big effects on the concentrations concentrations as seen in Figure 6. Everything still seems to evolve in the same way and stay in the same "balance". However, bigger changes can probably be seen by adding more reactions, but due to time constraints I did not have time to do so.

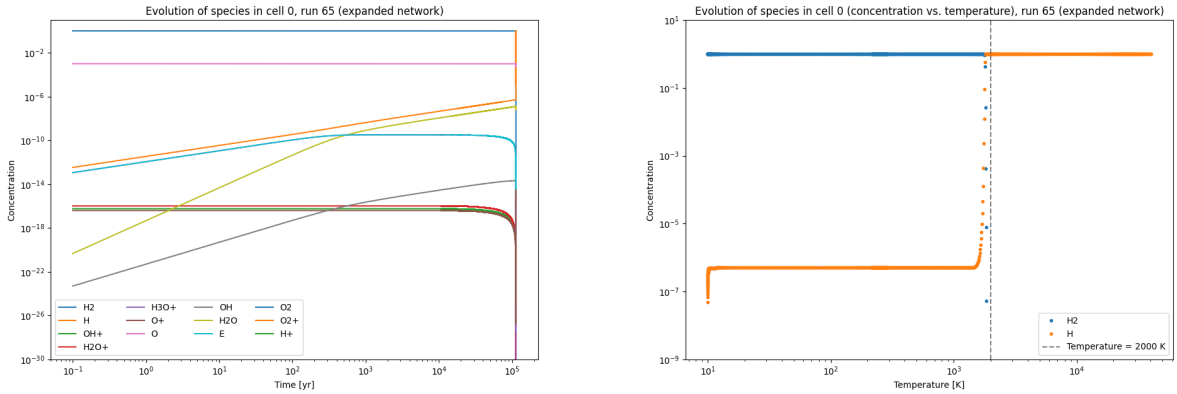

Figure 6: Different plots showing the expanded chemical evolution from run 67.

4 Conclusion & next steps

This simple chemical network simulates the evolution of different chemical species during early star formation and manages to capture some key processes (including the transition from the first to the second Larson core) that govern the formation and destruction of the species. The next step would be to expand the chemical network even further, to gain a better understanding of early star formation. Further work could also include making the code faster, perhaps by getting rid of the loops and/or experiment with parallelization.

References

[1] KIDA Collaboration. *The KIDA Chemical Database*. https://kida.astrochem-tools.org/. Accessed: 2025-01-15. Accessed 2025-01-15.

[2] Toyoharu Umebayashi and Takenori Nakano. "Magnetic flux loss from interstellar clouds". In: 243 (Mar. 1990), pp. 103–113. DOI: 10.1093/mnras/243.1.103.

[3] N. Vaytet and T. Haugbølle. "A grid of one-dimensional low-mass star formation collapse models". In: *Astronomy amp; Astrophysics* 598 (Feb. 2017), A116. ISSN: 1432-0746. DOI: 10.1051/0004-6361/201628194. URL: http://dx.doi.org/10.1051/0004-6361/201628194.